Enhancement of the Superconducting Gap by Nesting in $CaKFe_4As_4$: A New High Temperature Superconductor

Daixiang Mou,[1,2] Tai Kong,[1,2] William R. Meier,[1,2] Felix Lochner,[3] Lin-Lin Wang,[1] Qisheng Lin,[1] Yun Wu,[1,2] S. L. Bud'ko,[1,2] Ilya Eremin,[3] D. D. Johnson,[1,2,4] P. C. Canfield,[1,2] and Adam Kaminski[1,2]

[1]*Division of Materials Science and Engineering, Ames Laboratory, Ames, Iowa 50011, USA*

[2]*Department of Physics and Astronomy, Iowa State University, Ames, Iowa 50011, USA*

[3]*Institut fur Theoretische Physik III, Ruhr-Universitat Bochum, 44801 Bochum, Germany*

[4]*Department of Materials Science and Engineering, Iowa State University, Ames, Iowa 50011, USA*

(Received 17 June 2016; published 28 December 2016)

We use high resolution angle resolved photoemission spectroscopy and density functional theory with measured crystal structure parameters to study the electronic properties of $CaKFe_4As_4$. In contrast to the related $CaFe_2As_2$ compounds, $CaKFe_4As_4$ has a high T_c of 35 K at stochiometric composition. This presents a unique opportunity to study the properties of high temperature superconductivity in the iron arsenides in the absence of doping or substitution. The Fermi surface consists of several hole and electron pockets that have a range of diameters. We find that the values of the superconducting gap are nearly isotropic (within the explored portions of the Brillouin zone), but are significantly different for each of the Fermi surface (FS) sheets. Most importantly, we find that the momentum dependence of the gap magnitude plotted across the entire Brillouin zone displays a strong deviation from the simple $\cos(k_x)\cos(k_y)$ functional form of the gap function, proposed by the scenario of Cooper pairing driven by a short range antiferromagnetic exchange interaction. Instead, the maximum value of the gap is observed on FS sheets that are closest to the ideal nesting condition, in contrast to previous observations in other ferropnictides. These results provide strong support for the multiband character of superconductivity in $CaKFe_4As_4$, in which Cooper pairing forms on the electron and the hole bands interacting via a dominant interband repulsive interaction, enhanced by band nesting.

DOI: 10.1103/PhysRevLett.117.277001

The superconducting mechanism in iron-based, high temperature superconductors is an important topic in condensed matter physics. One key question is whether the system should be described within a weak coupling BCS-type approach with a key role played by the interband repulsion between electron and hole bands, separated by the large momentum transfer or by a strong coupling approach with dominant short-range antiferromagetic (AF) fluctuations, described by the local exchange interaction [1–7]. The former scenario seemed consistent with experimental results from a number of iron pnictide superconductors [8], but was later challenged by the discovery of iron chalcogenide-based superconductors [9,10]. Theoretical progress in this field was inspired by the discovery of new materials in this family [11], from iron chalcogenide [12] to single-layer FeSe films [13]. Materials with different crystal or electronic structures are extremely useful and provide new insights for constructing global models of high temperature superconductivity in iron-based materials.

Recently, a new iron-based class of superconductors, $AeAFe_4As_4$ (Ae = Ca, Sr, Eu and A = K, Rb, Cs), were reported (generically referred to as $AeA1144$) [14,15]. Although the chemical composition of $AeA1144$ is the same as the intensively studied $(Ba,K)Fe_2As_2$ system, it has a different crystal structure type with Ae and A layers alternatively stacked between Fe_2As_2 layers. The crystallographically inequivalent position of the Ae and A atoms changes the space group from $I4/mmm$ to $P4/mmm$. A high transition temperature (T_c = 31–36 K) and stochiometric composition makes the $AeA1144$ family an ideal new platform to test existing theories and inspire new ones. Measurements of its electronic structure and the momentum dependence of its superconducting gap are of critical importance.

In this Letter, we investigate the band structure and momentum dependence of the superconducting gap of $CaKFe_4As_4$, with high resolution Angle Resolved Photoemission Spectroscopy (ARPES) and Density Functional Theory (DFT) using experimentally obtained crystal structure parameters. Unlike most other iron-based superconductors, $CaKFe_4As_4$ has a high T_c of 35 K at stoichiometric composition, which allows for the study of iron-based high temperature superconductivity in the absence of disorder caused by substitution. The Fermi surface consists of three hole pockets at the Γ point and two electron pockets at the M point. The hole pockets have significantly different diameters, which allow us to measure the superconducting gap for different values of the total momentum $\mathbf{k}$. We find that the superconducting gap is

nearly isotropic on each Fermi surface (FS) sheet, but has a significantly different value for each of the FS sheets. Indeed, the largest superconducting gap is found for pairs of hole and electron pockets that have a similar diameter, while other pockets have a smaller value of the superconducting gap. This observation is in stark contrast to the situation in some other ferropnictides. For example, in LiFeAs, which is another stoichiometric pnictide superconductor with multiple FS sheets, the largest superconducting gap is found on the smallest hole pocket, located near the zone center [16,17]. Therefore, our results on $CaKFe_4As_4$ provide a new important ingredient that must be included in the superconducting mechanism of iron-based superconductors.

$CaKFe_4As_4$ single crystals were grown using the flux method and extensively characterized by thermodynamic and transport measurements [15,18]. The experimental structure parameters were obtained from single-crystal x-ray diffraction. Technical details are provided in the Supplemental Material [19]. Single-phase samples were cleaved *in situ* at a base pressure of lower than 8×10^{-11} Torr. ARPES measurements were performed using a tunable vacuum ultraviolet laser spectrometer [27] ($h\nu = 6.7$ eV, $\Delta E = 4$ meV) and helium microwave plasma spectrometer ($h\nu = 21.2$ eV, $\Delta E = 8$ meV). Assuming that $CaKFe_4As_4$ has the same inner potential (~12 eV) as $(Ba, K)Fe_2As_2$, then 6.7 eV and 21.2 eV light sources measure the electronic structure around $k_z = \pi$ and $k_z = 0$, respectively [28,29]. The energy corresponding to the chemical potential was determined from the Fermi edge of a polycrystalline Au reference in electrical contact with the sample. The consistency of the data was confirmed by measuring six different samples.

The measured FS and band dispersion are shown in Fig. 1. In data collected using a photon energy of 6.7 eV, three hole pockets are observed at the center of the zone [α, β, and γ, shown in panels (a)–(d)]. Whereas the α pocket is fairly round, the shapes of the β and γ pockets are more squarish. The approximate diameters of these three pockets are $\sim 0.2\pi/a$, $\sim 0.4\pi/a$, and $\sim 0.8\pi/a$, respectively. The FS and band structure data, measured using a photon energy of 21.2 eV, are shown in Fig. 1(e)–1(h). At this photon energy, only the largest hole pocket around Γ is observed, and its diameter is $\sim 0.45\pi/a$. The β pockets are not visible, most likely due to unfavorable matrix elements. The band responsible for α hole pocket is located 30 meV below E_F for this value of k_z [Fig. 1(g)]. This is consistent with the 3D character of most inner hole pockets in 122 systems [28,30]. We note that this change is not due to an increased sensitivity at low photon energies—in such a situation, two copies of the α band would be observed, one below and one above E_F, which is not the case. At the zone corner, a shallow electron FS pocket (δ) is observed [Fig. 2(g)–2(h)].

The Fermi surface and orbitally resolved band dispersion were calculated using DFT and a Local Density

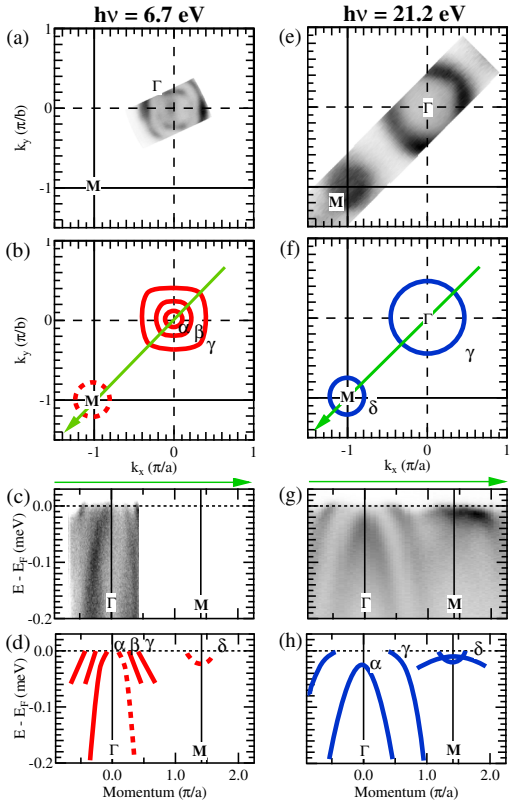

FIG. 1. Measured electronic structure of $CaKFe_4As_4$. (a) Fermi surface (FS) intensity acquired using photon energy of 6.7 eV at $T = 40$ K. (b) Sketch of the FS based on data in (a). (c) Measured ARPES intensity along a cut through the Γ point. Cut position is indicated in panel (b). (d) Sketch of the band structure based on data in (c). (e)–(h) Same as (a)–(d), but measured using a photon energy of 21.2 eV. Dashed lines in (b) and (d) mark the expected parts of the bands and FS that are not observed due to matrix elements and limited access to Brillouin zone at low photon energy.

Approximation (LDA) combination with experimental lattice constants and atomic positions (obtained from single-crystal x-ray diffraction measurements and shown in Table II of the Supplemental Material [19]). The resulting FS and band structure are shown in Fig. 2. The

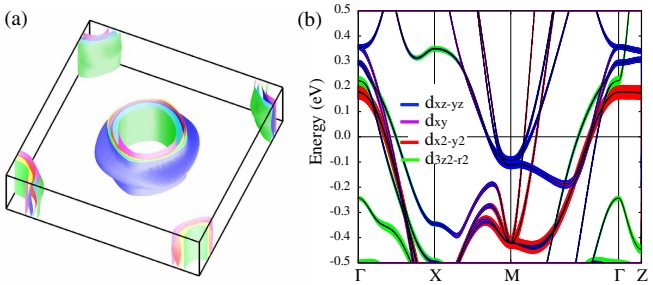

FIG. 2. (a) Calculated 3D Fermi surface of $CaKFe_4As_4$ (b) Band dispersion along the key symmetry directions with respective orbital contributions marked by color-coded outlines.

calculation predicts six hole pockets—slightly deformed, quasi 2D cylinders centered at the Γ point of the Brillouin zone, yet the ARPES data in Fig. 1 show only three Fermi sheets around Γ. Most likely, the intensity of the β sheet is due to three closely located bands that cannot be resolved experimentally. As in many other iron based superconductors, there are several $3d$ orbitals contributing to the states near the Fermi level. Figure 2(b) shows the band dispersion with color-coded orbital contributions. Most importantly, in $CaKFe_4As_4$, in addition to the yz/xz and x^2-y^2-orbital contributions to the FS pockets, there is also a strong admixture of $3z^2-r^2$ states to the α and γ bands, which is somewhat different from the other ferropnictides. In particular, the contribution of the $3z^2-r^2$ orbital to the states near E_F depends sensitively on the Fe ionic positions, as the latter are located at the off high-symmetry points in $CaKFe_4As_4$. In fact, in this system, there are two Fe-As distances in the As-Fe-As layer, which is in contrast to other ferropnictides such as LiFeAs and $CaFe_2As_2$. The calculation predicts four electron pockets centered at the M point. Experimentally, only one pocket can be resolved due to a significant intrinsic linewidth and the fact that the bottom of these bands is located very close to E_F.

Figures 3(a)–3(d) show the measured electronic structure at several typical temperatures along a cut near the Γ point. Because of matrix elements, only the β and γ bands are seen in this cut. Both bands show a clear backbending structure at low temperature [Fig. 3(a)]. We plot the Energy Distribution Curves (EDCs) at the k_F for several different temperatures in Fig. 3(e). A sharp quasiparticle peak gradually forms as the temperature is decreased below T_c. We symmetrized the EDCs at k_F, as shown in Fig. 3(f)–3(j), prior to performing fitting [31,32]. A BCS-based, phenomenological model [33] is used to fit the EDCs and extract the gap size. Results are shown in Fig. 3(j)–(k). All gaps follow a BCS-like temperature dependence and close at T_c, with $\Delta_{\alpha 0}=10.5$ meV, $\Delta_{\beta 0}=13$ meV, $\Delta_{\gamma 0}=8$ meV, and $\Delta_{\delta 0}=12$ meV, which gives rise to the ratio of $2\Delta_0/k_BT_c$ of 7.4, 9.1, 5.6, and 8.4, indicating that the superconductivity of $CaKFe_4As_4$ is in the strong coupling regime.

We measured the momentum dependence of the superconducting gap on the β and δ FS sheets, as summarized in Fig. 4, to elucidate the symmetry of the order parameter in $CaFeK_4As_4$. For qualitative analysis, we extract the EDCs at different k_F on the β and δ FS sheets and symmetrize them in Figs. 4(a) and 4(b). All symmetrized EDCs show a clear dip structure at E_F, and the energy positions of the quasiparticle peaks do not show much variation with the FS angle. In Fig. 4(c), we plot the extracted values of the superconducting gap as a function of FS angle. The gap sizes on these two FS pockets have no clear nodes and are roughly isotropic, which directly excludes the possibility of d-wave paring symmetry in $CaFeK_4As_4$ superconductor. In order to check the k_z dependence of the superconducting

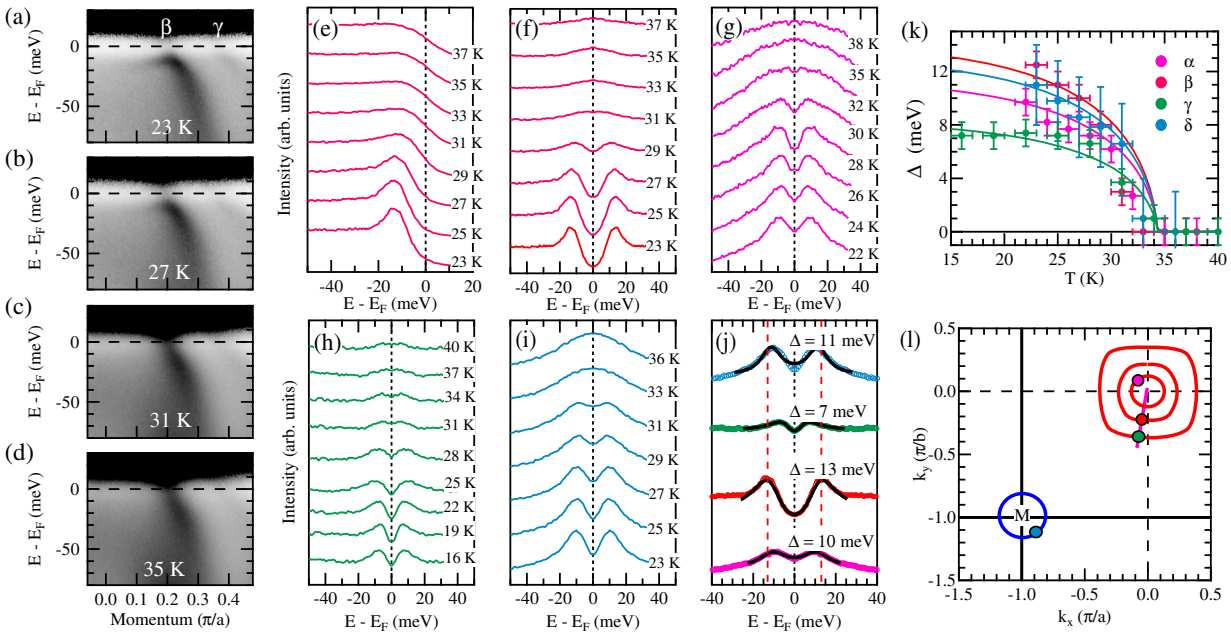

FIG. 3. (a)–(d) Measured electronic structure at four selected temperatures along the cut indicated in (l). The data is divided by the Fermi-Dirac function. (e) Energy Distributed Curves (EDCs) at k_F of β FS pocket. (f) The data from panel (e) after symmetrization. (g)–(i) Symmetrized EDCs at k_F of α, γ, and δ FS pockets, respectively. k_F positions are marked in (l). (j) Symmetrized EDCs at k_F for lowest measured temperature from (f)–(i). Red, vertical dashed lines mark the energy of largest gap (β FS sheet). The black lines are the fits using phenomenological model [33]. (k) Temperature dependence of the superconducting gaps for all four pockets. Solid lines are BCS predictions for Δ_0 of 10.5 meV, 13 meV, 8 meV, and 12 meV. (l) Sketch of the FS with indication of the cut position and k_F positions.

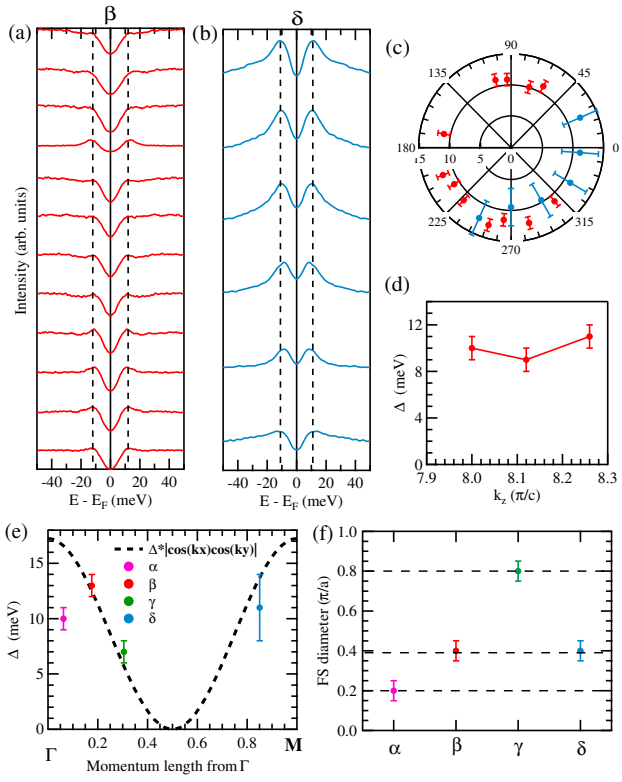

FIG. 4. Momentum-dependent superconducting gap. (a)–(b) Symmetrized EDCs at different k_F on the β and δ FS pockets. (c) Extracted superconducting gap from EDCs in (a) and (b). The Γ-X direction is set to 0 degree. (d) k_z dependence of superconducting gap on the β FS pocket. Data were taken with a photon energy of 5.7 eV, 6.2 eV, and 6.7 eV. Data in (a)–(d) were taken at 22 K. (e) Plot of the extracted gap on four FS sheets in Fig. 3(j) versus momentum distance from Γ. The black dashed line is a fit with the function $\Delta|\cos k_x \cos k_y|$, $\Delta = 16$ meV. (f) Measured diameters of four Fermi pockets.

gap, we measured the gap size on the β FS with three different photon energies that cover more than $0.2\pi/c$ in momentum space, as shown in Fig. 4(d). The gap size does not show much variation within this k_z momentum range either, indicating the quasi-2D nature of $CaFeK_4As_4$.

With the measured amplitude of superconducting gap on all four FSs of $CaFeK_4As_4$, we can now check the validity of the previously proposed gap functions. In the strong coupling approach [34,35], the pairing of electrons occurs because of a short-range interaction. If the antiferromagnetic exchange in iron-based superconductors is dominated by next-neighbor coupling (J_2) [5], the superconducting gap can be described by a single functional form in the entire BZ, given by $\Delta(k) = \Delta_0|\cos k_x \cos k_y|$ (or $|\cos k_x + \cos k_y|$ in the 2Fe per unit cell) [34]. Apparently, in this gap function, a FS sheet with a smaller diameter would have a larger superconducting gap around the BZ center, which is consistent with the measured gap size on the smallest hole pocket in several pnictide superconductors [8,36,37]. At the same time, another interpretation of this feature also exists in the purely band description of the $s^{\pm}$-wave superconductivity in which the large size of the superconducting gap on the smallest pocket is attributed to the dominant interband Cooper pair scattering between electron and hole bands of different sizes. In the absence of direct nesting, the magnitude of the gap is larger on that band, which has a smaller k_F [38,39]. In Fig. 4(e), we compare the measured gap sizes on different FS with a $\Delta_0|\cos k_x \cos k_y|$ function. The gap size on the α FS is much smaller than the value of the gap expected from the fit function (a ~15 meV gap size is needed to achieve a match). Therefore, the failure of applying the $\Delta_0|\cos k_x \cos k_y|$ function on our measured gap indicates that the superconductivity in $CaFeK_4As_4$ may not be immediately described within the short-range antiferromagnetic fluctuation model. Instead, the measured gaps are consistent with band description of supercondcutivity. In particular, in contrast to other ferrpnictides, some of the bands in $CaFeK_4As_4$ are nested; i.e., the β FS with the largest gap size among three-hole FS has the best nesting condition with the δ electron band FS [Fig. 4(f)]. It is known theoretically that the nesting between electron and hole bands enhances the repulsive interband interaction between them [1]. Once this interaction becomes larger than the intraband ones, it favors $s^{\pm}$ symmetry of the superconducting gap, with gap magnitudes being maximal on the FSs that are maximally close to the AF instability, while other gaps on non-nested FSs will be smaller.

In the simple mechanism of the $s^{\pm}$ superconducting gap, driven by strong interband repulsion (which is much bigger than the intraband interaction due to nesting of the electron and hole bands), the superconducting gaps on each FS appear to be equal and opposite in sign. Once the intraband interactions and further FSs (not nested) are added, the superconducting gap equations acquire the matrix form, and the exact distribution of the gaps on each FS start to depend on various factors such as density of state, orbital content, etc. However, the analysis of these equations in the past [40–43] has shown that the largest gaps always appear on those FSs that show the largest tendency towards AF instability, which corresponds to nesting of electron and hole bands.

In many of the other iron-based superconductors, xz/yz orbitals contribute mostly to the hole and electron FSs near the Γ and M points, respectively. Within the $s^{\pm}$ scenario, the superconducting gaps appear to be maximal on these orbitals due to strong intraorbital (interband) nesting of the electron and hole pockets. There are, however, scenarios (including the s^{++}-wave mechanism [44]) in which nesting does not play an important role and which also predict the largest superconducting gaps to be on the xz/yz orbitals. One of our most important findings is that in the 1144 compound, there are not just xz/yz orbitals, but also z^2 and $x^2 - y^2$, which participate in the intraorbital interband nesting. This provides strong support in favor of the $s^{\pm}$

scenario of superconductivity, driven by nesting of the electron and hole bands.

In conclusion, we measured the electronic structure and values of the superconducting gap of a new member of iron arsenic high temperature superconductor—$CaKFe_4As_4$. We find the superconducting gap is nearly isotropic within the explored region of the BZ. The largest gap is observed on the β hole and δ electron sheets, which have very similar diameters, whereas the α and γ sheets have smaller values of the superconducting gap, as they have no electron counterparts of similar diameter. This strongly supports the multiband character of the $s^{\pm}$-wave symmetry of the superconducting gap in which the Cooper pairing forms on the electron and hole bands with strong interband repulsive interaction, enhanced by the nesting of the electron and hole bands.

Raw data from this manuscript are available through the link in Ref. [45].

We would like to thank Rafael Fernandes and Peter Orth for very useful discussions. This work was supported by the U.S. Department of Energy, Office of Science, Basic Energy Sciences, Materials Science and Engineering Division (sample growth, characterization and ARPES measurements). Ames Laboratory is operated for the U.S. Department of Energy by Iowa State University under Contract No. DE-AC02-07CH11358. I. E. was supported by the joint Agence Nationale de la Recherche (ANR) and the Deutsche Forschungsgemeinschaft (DFG) Grant No. ER463/8-1 and by the German Academic Exchange Service (DAAD PPP USA, Grant. No. 57316180). W. R. M. was supported by is supported by the Gordon and Betty Moore Foundation EPiQS Initiative (Grant No. GBMF4411)

[1] A. V. Chubukov, D. V. Efremov, and I. Eremin, Phys. Rev. B **78**, 134512 (2008).
[2] I. Mazin and J. Schmalian, Physica C (Amsterdam) **469**, 614 (2009).
[3] S. Graser, T. A. Maier, P. J. Hirschfeld, and D. J. Scalapino, New J. Phys. **11**, 025016 (2009).
[4] Q. Si, R. Yu, and E. Abrahams, Nat. Mater. **1**, 16017 (2016).
[5] J. Hu, B. Xu, W. Liu, N.-N. Hao, and Y. Wang, Phys. Rev. B **85**, 144403 (2012).
[6] D. S. Inosov, J. T. Park, A. Charnukha, Y. Li, A. V. Boris, B. Keimer, and V. Hinkov, Phys. Rev. B **83**, 214520 (2011).
[7] P. Richard, T. Qian, and H. Ding, J. Phys. Condens. Matter **27**, 293203 (2015).
[8] P. Richard, T. Sato, K. Nakayama, T. Takahashi, and H. Ding, Rep. Prog. Phys. **74**, 124512 (2011).
[9] D. Mou, L. Zhao, and X. Zhou, Front. Phys. **6**, 410 (2011).
[10] D. Liu *et al.*, Nat. Commun. **3**, 931 (2012).
[11] Y. Kamihara, T. Watanabe, M. Hirano, and H. Hosono, J. Am. Chem. Soc. **130**, 3296 (2008).
[12] J. Guo, S. Jin, G. Wang, S. Wang, K. Zhu, T. Zhou, M. He, and X. Chen, Phys. Rev. B **82**, 180520 (2010).
[13] Q.-Y. Wang *et al.*, Chin. Phys. Lett. **29**, 037402 (2012).
[14] A. Iyo, K. Kawashima, T. Kinjo, T. Nishio, S. Ishida, H. Fujihisa, Y. Gotoh, K. Kihou, H. Eisaki, and Y. Yoshida, J. Am. Chem. Soc. **138**, 3410 (2016).
[15] W. R. Meier, T. Kong, U. S. Kaluarachchi, V. Taufour, N. H. Jo, G. Drachuck, A. E. Böhmer, S. M. Saunders, A. Sapkota, A. Kreyssig, M. A. Tanatar, R. Prozorov, A. I. Goldman, F. F. Balakirev, A. Gurevich, S. L. Bud'ko, and P. C. Canfield, Phys. Rev. B **94**, 064501 (2016).
[16] S. V. Borisenko, V. B. Zabolotnyy, A. A. Kordyuk, D. V. Evtushinsky, T. K. Kim, I. V. Morozov, R. Follath, and B. Büchner, Symmetry (Basel) **4**, 251 (2012).
[17] K. Umezawa, Y. Li, H. Miao, K. Nakayama, Z.-H. Liu, P. Richard, T. Sato, J. B. He, D.-M. Wang, G. F. Chen, H. Ding, T. Takahashi, and S.-C. Wang, Phys. Rev. Lett. **108**, 037002 (2012).
[18] T. Kong, W. R. Meier, F. F. Balakirev, S. L. Bud'ko, A. Gurevich, and P. C. Canfield, arXiv:1606.02241.
[19] See Supplemental Material http://link.aps.org/supplemental/10.1103/PhysRevLett.117.277001, which includes Refs. [20–26] for experimental details about determination of crystal structure parameters from x-way scattering measurements.
[20] Bruker, SAINT plus. version 8.30, Bruker AXS Inc., Wisconsin, USA (2013).
[21] G. M. Sheldrick, SADABS, University of Grottingen, 1996.
[22] Bruker, SMART for Windows NT/2000, version 6.148, Bruker AXS Inc., 2002.
[23] V. Petricek, M. Dusek, and L. Palatinus, JANA2006, The crystallographic computing system Institute of Physics, 2006.
[24] L. Palatinus and G. Chapuis, J. Appl. Cryst. **40**, 786 (2007).
[25] B. Saparov, C. Cantoni, M. Pan, T. C. Hogan, W. R. Li, S. D. Wilson, K. Fritsch, M. Tachibana, B. D. Gaulin, and A. S. Sefat, Sci. Rep. **4**, 4120 (2014).
[26] K. Sasmal, B. Lv, B. Lorenz, A. M. Guloy, F. Chen, Y.-Y. Xue, and C. W. Chu, Phys. Rev. Lett. **101**, 107007 (2008).
[27] R. Jiang, D. Mou, Y. Wu, L. Huang, C. D. McMillen, J. Kolis, H. G. Giesber, J. J. Egan, and A. Kaminski, Rev. Sci. Instrum. **85**, 033902 (2014).
[28] C. Liu, T. Kondo, N. Ni, A. D. Palczewski, A. Bostwick, G. D. Samolyuk, R. Khasanov, M. Shi, E. Rotenberg, S. L. Bud'ko, P. C. Canfield, and A. Kaminski, Phys. Rev. Lett. **102**, 167004 (2009).
[29] T. Shimojima *et al.*, Science **332**, 564 (2011).
[30] R. S. Dhaka, C. Liu, R. M. Fernandes, R. Jiang, C. P. Strehlow, T. Kondo, A. Thaler, J. Schmalian, S. L. Bud'ko, P. C. Canfield, and A. Kaminski, Phys. Rev. Lett. **107**, 267002 (2011).
[31] M. R. Norman, H. Ding, M. Randeria, J. C. Campuzano, T. Yokoya, T. Takeuchi, T. Takahashi, T. Mochiku, K. Kadowaki, P. Guptasarma, and D. G. Hinks, Nature (London) **392**, 157 (1998).
[32] T. Kondo, R. Khasanov, T. Takeuchi, J. Schmalian, and A. Kaminski, Nature (London) **457**, 296 (2009).
[33] H. Matsui, T. Sato, T. Takahashi, S.-C. Wang, H.-B. Yang, H. Ding, T. Fujii, T. Watanabe, and A. Matsuda, Phys. Rev. Lett. **90**, 217002 (2003).
[34] J. Hu and H. Ding, Sci. Rep. **2**, 381 (2012).
[35] Z. P. Yin, K. Haule, and G. Kotliar, Nat. Phys. **10**, 845 (2014).

[36] H. Ding, P. Richard, K. Nakayama, K. Sugawara, T. Arakane, Y. Sekiba, A. Takayama, S. Souma, T. Sato, T. Takahashi, Z. Wang, X. Dai, Z. Fang, G. F. Chen, J. L. Luo, and N. L. Wang, Europhys. Lett. **83**, 47001 (2008).
[37] L. Zhao, H.-Y. Liu, W.-T. Zhang, J.-Q. Meng, X.-W. Jia, G.-D. Liu, X.-L. Dong, G.-F. Chen, J.-L. Luo, N.-L. Wang, W. Lu, G.-L. Wang, Y. Zhou, Y. Zhu, X.-Y. Wang, Z.-Y. Xu, C.-T. Chen, and X.-J. Zhou, Chin. Phys. Lett. **25**, 4402 (2008).
[38] X. Chen, S. Maiti, A. Linscheid, and P. J. Hirschfeld, Phys. Rev. B **92**, 224514 (2015).
[39] A. V. Chubukov, I. Eremin, and D. V. Efremov, Phys. Rev. B **93**, 174516 (2016).
[40] P. J. Hirschfeld, M. M. Korshunov, and I. I. Mazin, Rep. Prog. Phys. **74**, 124508 (2011).
[41] S. Maiti, M. M. Korshunov, T. A. Maier, P. J. Hirschfeld, and A. V. Chubukov, Phys. Rev. B **84**, 224505 (2011).
[42] A. V. Chubukov, Annu. Rev. Condens. Matter Phys. **3**, 57 (2012).
[43] F. Ahn, I. Eremin, J. Knolle, V. B. Zabolotnyy, S. V. Borisenko, B. Büchner, and A. V. Chubukov, Phys. Rev. B **89**, 144513 (2014).
[44] H. Kontani and S. Onari, Phys. Rev. Lett. **104**, 157001 (2010).
[45] See http://lib.dr.iastate.edu/ameslab datasets/.